Proceedings of the 1st Marine Energy Technology Symposium
METS13
April 10-11, 2013, Washington, D.C.

AUGMENTING ENERGY EXTRACTION FROM VORTEX INDUCED VIBRATION USING STRIPS OF ROUGHNESS/THICKNESS COMBINATIONS

Ashwin Vinod[1] , Amshumaan Kashyap[2], Arindam Banerjee[1,*] and Jonathan Kimball[2]

[1]Department of Mechanical Engineering & Mechanics
Lehigh University, Bethlehem, PA 18015
[2]Department of Electrical & Computer Engineering
Missouri University of Science & Technology, Rolla, MO 65409
[*]Corresponding Author: Email: arb612@Lehigh.edu

ABSTRACT

The current work focuses on augmenting vortex induced vibration (VIV) of an elastically mounted circular cylinder, by using strips of roughness/thickness combination attached to its outer surface. Our main objective is to identify roughness/thickness configurations on cylinder which would lead to high amplitude vibrations and a greater synchronization range for the purpose of harvesting marine hydrokinetic energy. Sandpaper strips ranging from very fine to extra coarse macro grits (ISO/FEPA designations) were used to study the effect of distributed roughness on VIV of a circular cylinder. Increased vibration amplitudes and synchronization range were observed for the configurations with roughness. The response also showed a dependence on the grit size. The effect of position of the strip was studied by placing zero roughness strips at different angular positions from the upstream (frontal) stagnation point. A change in the response profile compared to the case of the smooth cylinder was observed. The response profiles of the configurations with the sandpaper strips and the zero roughness strips were compared in an attempt to decouple the effect of roughness and thickness and showed different response characteristics within different ranges of reduced velocities. Roughness experiments were repeated with springs of different stiffness, and variation in the synchronization range and vibration amplitudes was observed. Configurations that could lead to increased vibration amplitudes and synchronization range that would augment energy harvesting were found. The preferred power take-off (PTO) technology for our device is a tubular linear interior permanent magnet (TL-IPM) generator, used previously for wave energy convertor. Our VIV device has a similar oscillating motion, but the vibrational characteristics are significantly different. In particular, a key requirement is to minimize the effective mass added to the vibrating cylinder. A TL-IPM may be optimized for minimal translating mass and has very few moving components.

NOMENCLATURE

A	amplitude of vibration (m)
B_g	gap flux density (Wb/m^2)
B_t	tooth flux density (Wb/m^2)
C	coefficient of damping (Ns/m)
D	diameter of the cylinder (m)
D_m	diameter of the magnet (m)
f	frequency of vibration (Hz)
f_n	natural frequency (Hz)
F_{peak}	peak force acting on the cylinder(N)
f_{vo}	vortex shedding frequency (Hz)

k	spring constant (N/m)
L	length of the cylinder (m)
λ_m	peak flux linkage
m	oscillating mass (Kg)
m_a	added mass (Kg)
P	number of pole pairs
P_{avg}	average power output (watts)
R_{em}	emulated resistance (ohms)
U	free stream velocity (m/s)
υ	kinematic viscosity (m^2/s)
ρ	density of water (Kg/m^3)
τ	pole pitch
ζ_e	effective damping

INTRODUCTION

Many recent scientific studies[1, 2] have emphasized the need for an environment friendly, low cost, renewable energy technology to mitigate the current rate of fossil fuel usage and their ensuing effects of climatic changes and global warming. Since the fossil fuel reserves are limited and may not last beyond the current century [3], efforts for development of alternate energy resources that are sustainable and environmentally friendly has been the focal point of research of many private companies[4-7] and federal research agencies[8-10]. An emerging resource is marine hydrokinetic (MHK) energy which uses ocean waves or river/tidal currents to harness hydro kinetic energy: the concept is fundamentally different from traditional hydropower which requires construction of a dam and has significant start-up costs. MHK systems are typically classified into: (a) *Rotary systems* (turbines) – some examples being tidal, river or marine current turbines from RoTech [11], Verdant Power [5] and Seagen[12]; and (b) *Non-rotary* or *oscillating systems* that behave like point or line absorbers – some examples being Oscillating water column [13], OPT's Power Buoy [14] and Pelamis[15].

A novel concept of using vortex induced vibration (VIV) for energy generation was invented in 2005 by Prof. Michael Bernitsas and co-workers and has been patented through the University of Michigan[16]. The system is named VIVACE – Vortex induced Vibration for Aquatic Clean Energy[4, 17-20]. Traditionally VIV has been considered to be destructive in nature and engineering solutions have been developed to suppress the destructive phenomena. The concept of power generation from VIV is unique as it breaks from tradition to "enhance" vortex shedding under significant damping rather than suppressing it [18]. The device is simple in construction and has no rotating parts; additionally, it is modular, scalable, robust, and environmentally (fish) friendly as the phenomena of vortex shedding from the device is identical to the method used by schools of fish to propel themselves. Thus, a problem with fish strikes that may be of concern to environmental agencies for rotary systems is not present in the VIV based system. The VIVACE generates electrical energy utilizing free vibration of oscillating cylinders in a fluid flow and uses a complex power take-off (PTO) mechanism using gears and cams[18, 19].

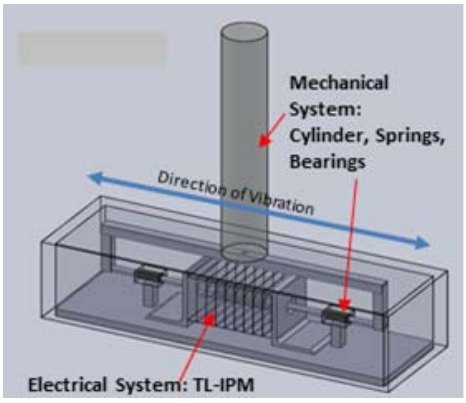

FIGURE 1. CONCEPTUAL DESIGN OF THE eVIV SYSTEM

Our system, which we call "*e-VIV*" (enhanced Vortex Induced Vibration), is different from VIVACE as we use a Tubular Linear Interior Permanent Magnet (TL-IPM) generator that is chosen to minimize mechanical components and reduce any subsequent parasitic losses. Figure 1a shows a schematic of the e-VIV system. The cylinder for our system is mounted vertical to the river/ocean bed, hence would enable deployment in shallow streams; the VIVACE is mounted horizontal to the river/ocean surface[19]. In addition, we employ innovative vibration enhancement techniques by using strips with zero to moderate roughness to enhance the amplitude of vibration and hence the power output from the device. The enhancement is similar in technique to the work done by the Bernitsas group [18, 20], however, our experiments explore a wider range of parameter space in terms of roughness, stiffness and location of the strips. The current work focuses on augmenting vortex induced

vibration (VIV) of an elastically mounted circular cylinder, by using roughness strips attached to its outer surface. Our main objective is to identify cylinder configurations which would lead to high vibration amplitudes and a greater synchronization range (range of velocities over which significant vibrations exist) for the purpose of harvesting marine hydrokinetic energy.

PHYSICS OF VIV

To illustrate the physics of VIV, we consider the experimental configuration that has been used in our laboratory (see fig.2a). The configuration is similar to the classical VIV experiments described by Khalak and Williamson[21]. A rigid cylinder is subjected to a uniform cross-flow of water and is allowed to vibrate in the transverse direction only, through springs. The characteristics of the cylinder are its diameter D, length L and mass m. As the flow velocity is increased, the motion of the cylinder is analyzed in terms of its amplitude (A) and the frequency spectrum. Two essential dynamic features are observed, as seen in Fig.2b and 2c: a significant oscillatory motion about one diameter in amplitude is observed over a limited range of velocities associated with a significant change in frequency. It is well known that one of the frequencies present in the spectrum is due to the flow oscillations in the wake [22-24]. Vortex shedding is thus a direct measure of the nature of flow dynamics associated with a vibrating entity and has been widely studied for an oscillating, elastically mounted cylinder[25]. Wake patterns induced by the vibration of the body can be classified into three primary modes of vibration[26], namely the 2S, 2P and P + S modes, where S stands for a single vortex and P for a pair of vortices (see Fig. 3). In the 2S mode (2 Single Vortices), there are two counter rotating vortices shed for one oscillation of the vibrating body (like the classic Karman vortex street). In the 2P mode (2 Pair Vortices), there are two pairs of counter rotating vortices shed per cycle of the vibrating body. Forced vibration can also lead to other vortex modes including the P+S mode (1 Pair + 1 Single Vortex), which is <u>not</u> able to excite a body into free vibration. A periodic vibration is observed if the energy transfer from the fluid to the body over a cycle is positive. This net energy transfer is influenced significantly by the timing of the vortex dynamics. VIV is therefore a fascinating coupling between body motion and vortex motion and many fundamental questions remain unanswered, particularly for the present application where we wish to enhance VIV.

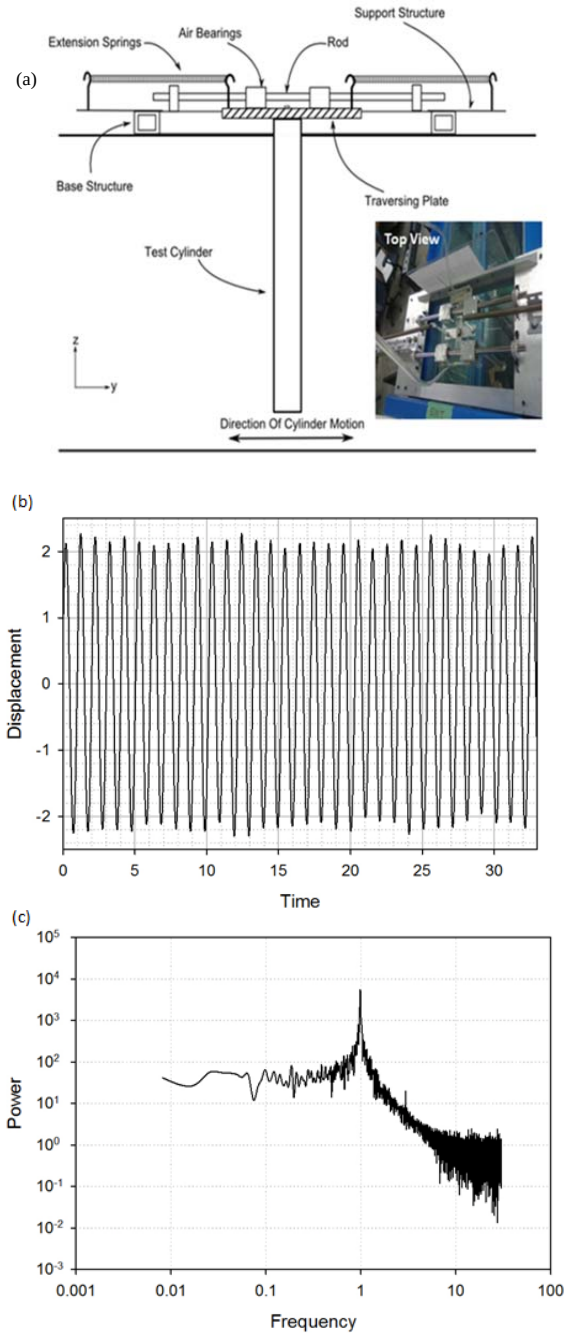

FIGURE 2. (A) SCHEMATIC OF ELASTICALLY SUPPORTED RIGID CYLINDER IN CROSS FLOW (INSET) – TOP VIEW OF MECHANICAL ARRANGEMENT THAT WAS MOUNTED ON A WATER TUNNEL, (B) DISPLACEMENT (A*=A/D) VS. TIME PLOT FOR A CYLINDER (D = 0.04826 M) AT RESONANCE (F_N= 0.9 HZ), (C) POWER SPECTRAL DENSITIES VS. FREQUENCY FOR (B).

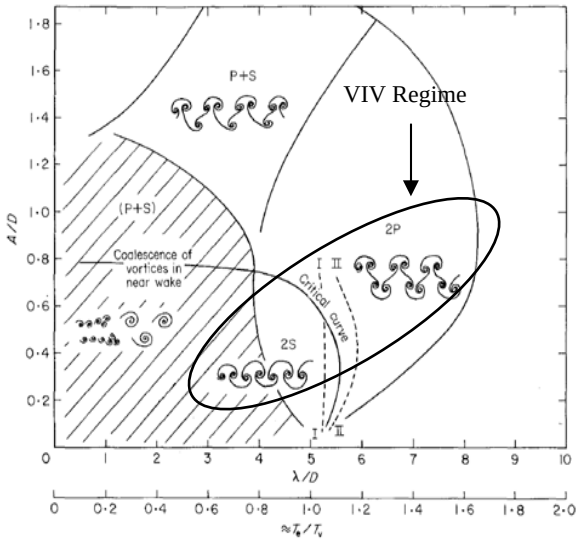

FIGURE 3. MAP OF VORTEX SYNCHRONIZATION PATTERNS NEAR THE FUNDAMENTAL LOCK-IN REGION[26]. VIV OCCURS TYPICALLY BETWEEN THE 2S AND THE 2P REGIME

EQUATION OF MOTION:

The spring-mass system can be analyzed based on the theory of free vibrations of elastically supported rigid cylinders. For the spring-mass system under consideration here, the primary (dominant) response mode is transverse to the flow and the governing equation describing the motion of the vibrating body is:

$$m\ddot{y} + c\dot{y} + ky = F(t) = F_L \sin(\omega t + \phi) \quad (1)$$

where *F(t)* is the hydrodynamic forcing, $m\ddot{y}$ is the body force, $c\dot{y}$ the damping force and *ky* the spring force acting on the rigid body. For small oscillations at the synchronous range, a good approximation of the transverse force is given by a sinusoid at the vortex shedding frequency such that F_L is the lift force acting on the cylinder due to the vortex shedding from the surface and ϕ is the phase angle between the fluid force and body displacement. Both of these components are crucial in determining the energy transfer from the working fluid to the bluff body and thus influence the amplitude of oscillation[27-29]. For the interest of the reader, traditional non-dimensional parameters that are often used in the study of VIV and that will be used repeatedly throughout this paper are provided in Table 1.

TABLE 1. NON DIMENSIONAL PARAMETERS

Mass Ratio	m^*	$4m/\pi\rho D^2 L$
Damping Ratio	ζ	$c/2\sqrt{k(m+m_a)}$
Reduced Velocity	U^*	$U/f_n D$
Amplitude Ratio	A^*	A/D
Frequency Ratio	f^*	f/f_n
Reynolds Number	Re	UD/υ
Strouhal Number	St	Df_{vo}/U

METHODS

All experiments were performed using a Water Tunnel facility (Model No. 1520 Rolling Hills Research, CA), which is 0.381 meters (15 inches) wide, 0.508 meters (20 inches) deep and 1.524 meters (60 inches) long and has a free surface test section. The water tunnel has an overall volumetric capacity of approximately 1000 gallons. The maximum flow velocity that can be attained in the test section is about 0.91 m/s (3 ft/sec). However, the maximum velocity used for the reported experiments was 0.58 m/s (23 inch/sec). The Reynolds number for each experiment varied between 3×10^3 and 3×10^4. The experimental setup (see Figure 2a) is primarily composed of an aluminum frame, a Plexiglas traversing plate, air bearings, mounting blocks, steel rods, indicator pin, custom made extension springs and the cylinder. More details can be found elsewhere[30, 31].

The cylinder used for the experiments was made of PVC pipe (with acrylic end caps) of diameter 0.04826m (1.9") and was 0.508m (20") long. The mass ratio (*m**) of the oscillating system used is 1.53. Air bearings (Newway Inc.) were used to minimize frictional damping; an operating pressure of 80 psig was maintained for all the experiments. Four sets of extension springs (W.B. Jones Springs), of stiffness, 1.015N/m, 6.3N/m, 45.4N/m and 84.026N/m were used for the stiffness experiments. Stainless Steel rods (0.5" dia) having a diameter tolerance of -0.0005" to -0.001" were used to mate with the bearing and allow transverse motion.

In order to study the effects of roughness and position, sandpaper strips 0.5" wide and 20" long were used. The details of the sandpaper strips and the zero roughness strips used are given in Table 2.

TABLE2: ISO/FEPA DESIGNATIONS OF STRIPS USED

Strip Used	Total Size (microns)	Average Grain size (microns)	Base Size (microns)
Zero Roughness	787	0	787
P36	1570	538	1040
P60	864	269	595
P320	432	46.2	386

A high speed camera (Photron FASTCAMX, Model No.1024 PCI) was used to capture the response behavior of the system at a rate of 60 frames/sec. Image analysis was done in MATLAB to obtain the displacement and frequency values of the system.

RESULTS

Effect of Roughness

A series of experiments were performed using strips listed in Table 2. The results obtained are plotted along with the case of a smooth cylinder. All the experiments reported in this section were performed by placing two strips, each at an angle of 60^0 from the stagnation point. Figure 4 shows one of the strips attached to the surface of the cylinder. From the experiments on the effect of position (reported in the following sub section), it was found that, the strips when placed at 60^0 (spanning the region within which the point of separation oscillates) dramatically altered the response profile of the cylinder and hence was chosen to study the effect of surface roughness.

FIGURE 4. CYLINDER WITH THE P60 STRIP ATTACHED AT 600 FROM THE STAGNATION POINT.

Figure 5(a) plots the amplitude response profile of the different cylinder roughness configurations. The traditional non-dimensional formulation given by Khalak and Williamson[21] is used to plot the amplitude ratio (A^*)and frequency ratio (f^*) as a function of the reduced velocity (U^*). The different amplitudes obtained in an experiment were sorted and the average of the maximum 10% of amplitudes (a common practice in the VIV community [20, 25, 32]) is plotted in figures 5a, 6a and 7a.

An increase in vibration amplitudes can be observed in case of configurations with the zero roughness as well as the three roughness strips. The front edge of the strips (when placed at 60^0) trips boundary layer separation in a controlled manner. This leads to straightening of the separation line and an increase in the span wise correlation and lift forces, thereby amplifying cylinder vibrations [17, 18, 33]. The amplitude response profile of the cylinder with strips attached to its outer surface was observed to be different from the traditional three branch response observed by Khalak and Williamson[34]. For a low mass damping system, Khalak and Williamson observed an initial excitation regime, an upper branch of response (high vibration amplitudes) and a lower branch of response. For a smooth cylinder, the initial branch typically exists within the reduced velocity range $4.0 \leq U^* \leq 5.5$, the upper branch within $5.5 \leq U^* \leq 9.8$, and the lower branch, within $10.7 \leq U^* \leq 12.2$. [20]

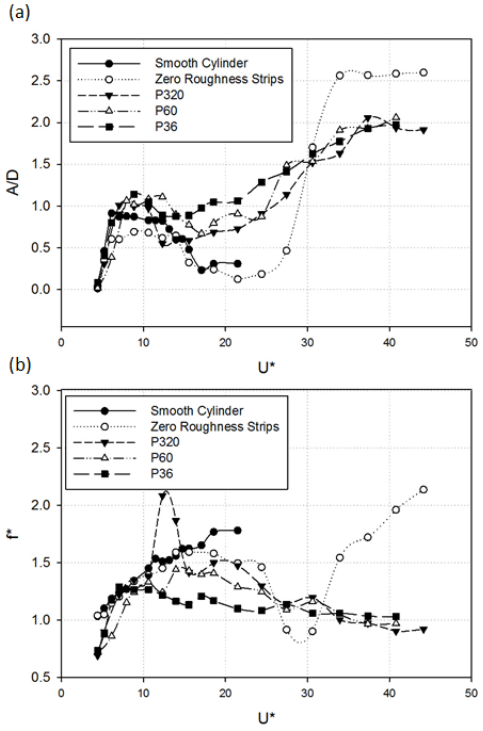

FIGURE 5. (A) AMPLITUDE RESPONSE PROFILES AND (B) FREQUENCY RESPONSE PROFILES SHOWING EFFECT OF ROUGHNESS (ζ = 0.04135)

In the current experiments with the roughness strips, the lower branch was not observed. The upper branch extended over a wider range of reduced velocity ($6 \leq U^* \leq 30$), and was followed

by a region of very high vibration amplitudes ($A/D \geq 1.5$). Due to absence of a suitable nomenclature for this branch in VIV literature, we refer to this region as a *super-upper branch.* The nature of response within the super-upper branch is similar to the galloping response observed by Chang et al.[20]. But further experimentation, like flow visualization and estimation of drag and lift coefficients are essential to quantitatively confirm galloping instability[35]. Similar high amplitude vibrations were observed also by Jubran et al.[36] and Bernitsas and Raghavan[18] in their experiments on flow induced vibration of circular cylinders with roughness strips. The vibration amplitudes of the smooth cylinder and the cylinder with roughness strips were comparable in range of reduced velocities $5 \leq U^* \leq 12$. For a value of U^* greater than 12, the smooth cylinder enters the lower branch with reduced vibration amplitudes whereas the configuration with the roughness strip continues to vibrate in the upper branch. Comparing the configuration with the roughness strips to that with the zero roughness, it can be seen that a cylinder with the zero roughness (strip) does have a lower branch of response following the upper branch, unlike the case of a cylinder with roughness strips. The vibration amplitudes for the cylinder with the zero roughness strips is consistently low compared to the case of the cylinder with the roughness strip until the value of $U^* \sim 30$. The increased amplitudes in this region could probably result from the eddies formed behind the roughness elements which add energy to the boundary layer and the vortices shed, which in turn amplify the fluctuating lift force and vibration amplitudes[33].

In the *super-upper branch* (U^*>~30), higher values of A/D were obtained for the configuration with the zero roughness strips as compared to the roughness strips. The strength of vortices shed increases with the amplitude of oscillation[29]; hence very strong vortices are expected to be shed from the cylinder when it vibrates in the *super-upper branch*. At these high velocities, eddies being shed from the roughness elements tend to smear the vortices compared to the case of the cylinder with the zero roughness strips. Smeared vortices are weaker in strength[20] and hence lead to comparatively reduced vibration amplitudes in case of configurations with the roughness strip.

The frequency response profiles for the different configurations are shown in figure 5(b) and clearly demonstrate the effect of roughness. It can be seen that as the reduced velocity increases (or as velocity of the flow increases) the frequency of vibration of the smooth cylinder keeps on increasing. The frequency profile of the configurations with the roughness strips increases with the reduced velocity up to a value of $U^* = 12$, then they begin to curve back downwards to the natural frequency of vibration in water. A similar observation was made by Chang *et al.*[20] in their experiments, where a sudden decline in the frequency response was observed with the onset of galloping. The frequency response of the configuration with the zero roughness strips is atypical. High frequency values were obtained at high reduced velocities and high vibration amplitudes contrary to expectation. Variations were observed in the response profiles with the roughness strips depending on the grit size of the sandpapers used. P36 is the largest in grit size, followed by P60 and P320 in order. Eddies shed from the grits are of the order of the dimension of the grits[33] as a result of which larger vortices being shed from P36 and P60 roughness strips result in higher vibration amplitudes over a wide range of reduced velocities.

Effect of Position

Experiments were performed using strips of zero roughness in order to study the effect of the position of the strip on VIV signature. The angle of separation for the flow around a circular cylinder has been widely studied by many researchers [37-42] in the past. To summarize, the angle of separation for a flow around a circular cylinder is oscillatory in nature and varies between 75^0 and 91.5^0 for Reynolds number between 10^4 and 10^7. For the current experiments, three different angular positions were selected to place the roughness strip, (1) before the region of natural separation (at 60^0), (2) within the region of natural separation (at 80^0) and, (3) beyond the region of natural separation (at 100^0). Chang et al.[20] also performed experiments to study the effect of different positions. They investigated positions in which the upstream location of the strips was varied from 20^0 to 64^0. The variation in response, depending on the position of P60 and P180 was presented in the PTC-to-FIM map by Park et al[43].

Figure 6 plots the amplitude and frequency response profiles showing the effect of position of the strip for a system employing a spring of stiffness 6.3 N/m. High amplitude ratios were obtained for the configuration with strips placed at 60^0. The strips when placed at 60^0 from the stagnation point, trip separation in a controlled manner, as they are ahead of the region within which the natural angle of separation oscillates. This leads to the straightening of the separation line, increasing the spanwise correlation and lift forces, consequently amplifying the vibrations [17, 18]. The supper upper branch was observed for this configuration for $U^* > 30$. The A/D values for the configurations with the strip at 80^0 and 100^0 were quite similar to the case of a smooth cylinder. An increase in the synchronization range was observed for configurations with the strips at 80^0, but the supper upper branch was not observed, whereas for the configuration with strips at 100^0, no noticeable change in the synchronization range was seen.

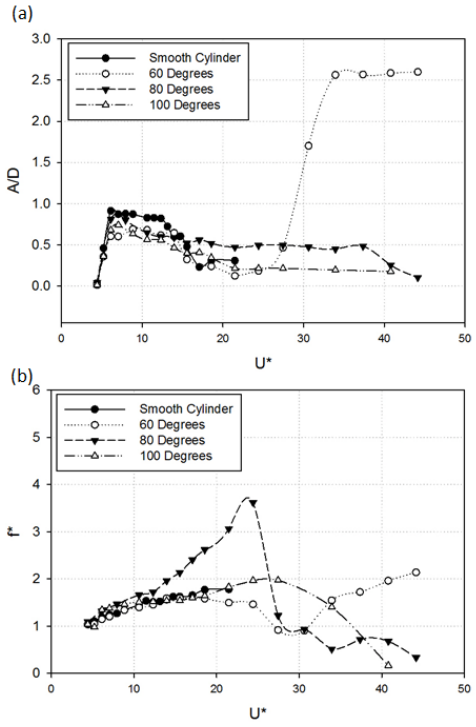

FIGURE 6. (A) AMPLITUDE RESPONSE PROFILES AND (B) FREQUENCY RESPONSE PROFILES SHOWING EFFECT OF POSITION (ς = 0.04135)

A variation was observed in the frequency response of the cylinder depending on the position of the strip (see Figure 6b). The smooth cylinder, configuration with strips at 80^0 and 100^0 showed increasing values of frequency with respect to the reduced velocity. The frequency response of the configuration with the strips at 60^0, showed a tendency to curve back downwards, to values close to the natural frequency in water as compared to the other configurations.

Effect of Stiffness

In addition to finding the effect of roughness and position, the effect of stiffness of the system was also investigated. The experiments were repeated using four different springs, of spring constants, 1.015N/m, 6.3N/m, 45.4N/m and 84.026N/m. The amplitude and frequency response profiles showing the effect of stiffness for the case of zero roughness strips at 60^0 are shown in Figure 7.

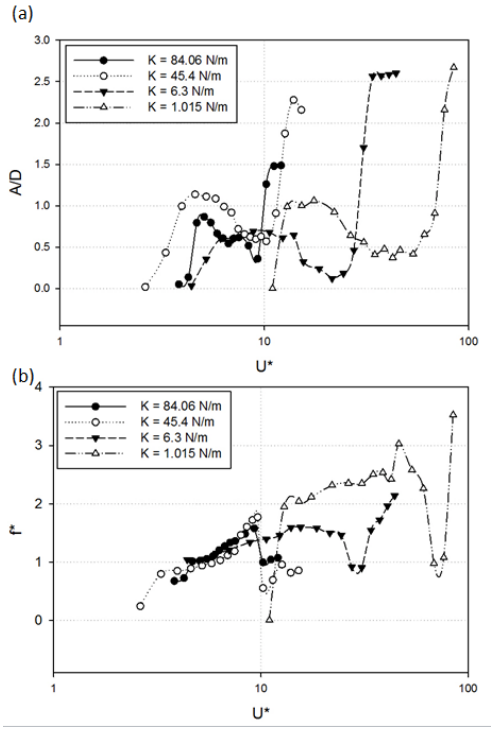

FIGURE 7. (A) AMPLITUDE RESPONSE PROFILES AND (B) FREQUENCY RESPONSE PROFILES SHOWING EFFECT OF STIFFNESS (ZERO ROUGHNESS STRIPS AT 60^0)

The most notable consequence of changing the stiffness was a change in the synchronization range. Reducing the stiffness of the spring led to an increase in the synchronization range. It was an expected result, primarily due to the formulation of the reduced velocity parameter ($U^*=U/f_nD$). The natural frequency (f_n) appearing in the denominator depends on the stiffness of the spring. Hence for a given value of free stream velocity, greater values of reduced velocity can be achieved by using spring of lower stiffness. Effect of stiffness on amplitude ratios of vibration was

also observed, but they were limited to the cases with strips placed at 60^0. Higher vibration amplitudes were observed within the supper upper branch with the less stiff springs, whereas the changes in the A/D values were not as conspicuous in the other regions.

The configurations with the strips at positions other than 60^0 degrees did not show a significant change in the response pattern. With a decrease in the spring constant of the spring used, a decrease in the frequency of vibration was observed. But the rate of decrease of the frequency of vibration was less than the rate of decrease of the spring constant values and natural frequency. Hence increasing values of frequency ratios were obtained with the less stiff springs as can be seen in figure 7.

ELECTROMECHANICAL SYSTEM

Whereas a turbine-based system for hydrokinetic energy extraction is compatible with rotary generators, the linear, oscillatory motion of a VIV system requires a different approach. To minimize the added mass of the generator, a tubular linear interior permanent magnet generator (TL-IPM) is used. There are a variety of tubular linear generator configurations. The Θ configuration (the Θ symbol indicates that the stator is longer than the translator and completely encloses it throughout its motion) of a TL-IPM, shown in Figure 8, minimizes translating mass.

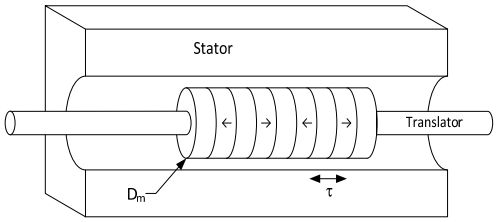

FIGURE 8. CONCEPTUAL DRAWING OF TL-IPM IN Θ CONFIGURATION.

The objective of the generator design is to produce maximum force for a given translating mass, and then to choose the design that matches the VIV prime mover. Nonlinear optimization methods and the models of[44] were used to find curves of maximum force density. As shown in Figure 9, regardless of the number of pole pairs (p), there is a curve that relates force density to the translator's aspect ratio. Furthermore, as shown in Figure 10, there is an optimal ratio between air gap flux density, B_g, and tooth flux density, B_t. If the translator volume is swept and p is varied, average force for a mass-optimal design may be found, as shown in Figure 11.

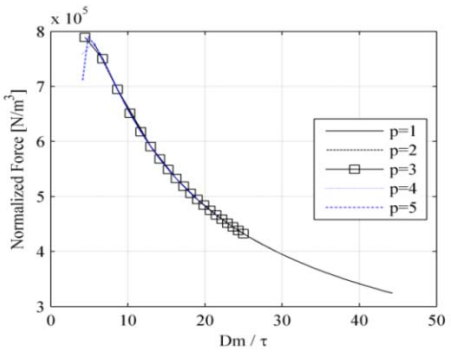

FIGURE 9. GENERATOR FORCE NORMALIZED TO TRANSLATOR VOLUME, VARIATION AS ASPECT RATIO OF TRANSLATOR POLES IS SWEPT.

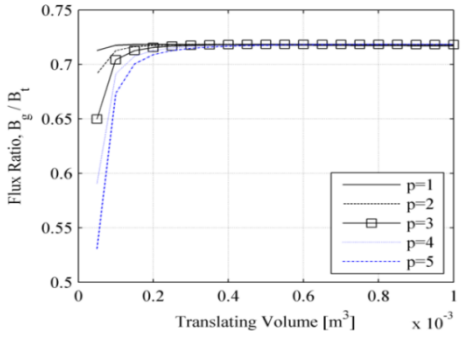

FIGURE 10. OPTIMAL RATIO BETWEEN AIR-GAP AND TOOTH FLUX DENSITIES AS TRANSLATOR VOLUME IS SWEPT FOR DIFFERENT NUMBER OF POLE PAIRS.

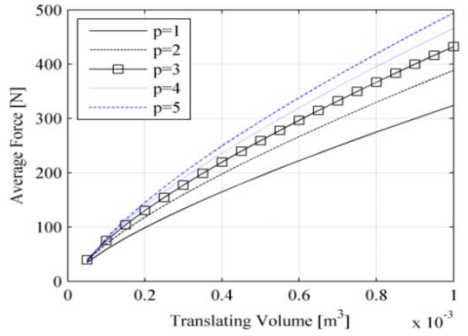

FIGURE 11. AVERAGE FORCE PRODUCED BY MASS-OPTIMAL TL-IPM FOR DIFFERENT POLE PAIRS AND TRANSLATING VOLUME.

In general, a design with more pole pairs corresponds to greater average force because the B_g/B_t and D_m/τ guidelines of Figures 9-10 govern the size of a given pole pair.

With a properly-designed generator, power may be extracted with a power converter controlled to behave like an emulated resistor, R_{em}. This is a common approach to energy harvesting in other

application domains, such as vibrational energy harvesting[45-47]. The effective damping constant with a given R_{em} is

$$\zeta_e = \frac{\pi\lambda_m^2}{2R_{em}A\tau}\left(\frac{\pi A}{\tau} + 2J_1\left(\frac{\pi A}{\tau}\right)\right) \quad (2)$$

where A is the amplitude of vibration, λ_m is the peak flux linkage, and J_1 is a Bessel function of the first kind. This is a complicated but monotonic relationship. Therefore, a conventional maximum power point tracking algorithm may be used, such as perturb & observe[48].

The peak force (F_{Peak}) acting on the cylinder and the average power (P_{avg}) for the proposed system are given by the following expressions:

$$F_{Peak} = AC\pi f \quad (3)$$

$$P_{avg} = \frac{F_{Peak}^2}{2C} \quad (4)$$

Therefore the contribution of the vibration amplitudes (A) on the average power output is evident. An increase in the vibration amplitudes by a factor of two, would lead to a fourfold increase in the power output.

CONCLUSION:

From the experimental results for the mechanical system of our e-VIV device, it can be clearly seen that the roughness/thickness configuration is significant in determining its amplitude and frequency response. Roughness, when selectively placed in the region within which the point of flow separation oscillates, increased the vibration amplitudes. The amplitudes also varied with the size of the roughness employed. The most interesting find, was the ability of the zero roughness strip to replicate the large amplitude response within the *super-upper branch*. This adds strength to the notion that the *super-upper* branch is more of a consequence of thickness and a weak function of roughness. The higher amplitude and frequency attained with the zero roughness strips, within the super-upper branch, could make it a better choice from an energy harvesting perspective. The position of strip with respect to the stagnation point is of pivotal importance and showed dramatic changes in the response profile at 60^0 whereas other positions (80^0 and 100^0) did not present a very conspicuous change. Experiments were also conducted to understand the effect of stiffness. A decrease in the stiffness of the spring resulted in an increase in the synchronization range and amplitude ratios, especially in the supper upper branch. Configurations were found that could augment VIV, wherefore increase energy extraction from VIV were found. Parametric studies were conducted with the electrical subsystem. A mass-optimal TL-IPM generator was designed to produce the correct force and guidelines for a preliminary optimization study were obtained. From a simple analytic evaluation of the expression for the power output, it can be seen that, a modification in the amplitudes by a factor of n, would modify the average power output by a factor of n^2, hence promising an effective approach to increased energy extraction. Our preliminary estimates indicate that the e-VIV system is more suitable for shallow flows where it is difficult to place rotary systems or in tidal basin where there is flow reversal (the design eliminates the need of expensive yaw mechanisms). Current experimental efforts are underway in integrating the mechanical and electrical subsystem for our e-VIV generator. Real time testing of the integrated system would be essential to uncover the harmful environmental effects (if any) of such a system.

ACKNOWLEDGEMENT:

The authors acknowledge support of the Office of Naval Research (Grant # ONR-000141210495, Program Manager: Ronald Joslin)

REFERENCES:

1. Tol, R., 2002, "Estimates of the damage costs of climate change: Benchmark Estimates." Environmental and Resource Economics, **21**: pp. 47-73.
2. Fankhauser, S. and Tol, R., *The social costs of climate change: The IPCC second assessment report and beyond*. 1997. p. 385-403.
3. Shaifee, S. and Topal, E., 2009, "When will fossil fuel reserves be diminished." Energy Policy, **37**: pp. 181-189.
4. www.vortexhydroenergy.com. *Vortex Hydro Energy*.
5. http://verdantpower.com/. *Verdant Power*.
6. http://hgenergy.com/index.php. *Hydro Green Energy*.
7. http://cleangt.com/home.html. *Greene Turbine, LLC*.
8. http://www.onr.navy.mil/. *Office of Naval Research (ONR)*.
9. http://www.nrel.gov/. *National Renewable Energy Laboratory*.
10. http://www.eere.energy.gov/. *U.S. Department of Energy - Energy Efficiency and Renewable Energy*.
11. Bahaj, A.S., 2007, "Experimental verification of numerical predictions for the hydrodynamic performance of horizontal axis marine current turbines." Renewable Energy, **32**: pp. 2479-2490.

12. Willden, R.H.J. and Graham, J.M.R., 2001, "Numerical prediction of VIV on long flexible circular cylinders." Journal of Fluids and Structures, **15**: pp. 659-669.
13. http://www.energetech.com/. *Oscillating Water Column*.
14. http://www.oceanpowertechnologies.com/. *O. P. Technologies*.
15. http://www.pelamiswave.com/. *Pelamis Wave Energy*.
16. Bernitsas, M.M. and Raghavan, K., *"Fluid Motion Energy Converter", United States Patent and Trademark Office, Patent US7493759,*2009.
17. Bernitsas, M.M., Raghavan, K., and Duchene, G. "Induced Separation and Vorticity using Surface Roughness in VIV of Circular Cylinders at $8x10^3$<Re<$2.1x10^5$"2008. in *Proceedings of ASME 27th International Conference on Offshore Mechanics and Arctic Engineering*. Estoril, Portugal.
18. Raghavan, K. and Bernitsas, M.M. "Enhancement of High Damping VIV through Roughness Distribution for Energy Harnessing at 8 X 10^3 < Re <1.5 X 10^5"2008. in *Proceedings of ASME 27th International Conference on Offshore Mechanics and Arctic Engineering*. Estoril, Portugal.
19. Bernitsas, M.M. and Raghavan, K., 2008, "VIVACE(Vortex Induced Vibration Aquatic Clean Energy): A New Concept in Generation of Clean and Renewable Energy from Fluid Flow." Journal of Offshore Mechanics and Arctic Engineering, **130**: pp. 041101.
20. Chang, C.C., Kumar, R.A., and Bernitsas, M.M., 2011, "VIV and galloping of single circular cylinder with surface roughness at 3.0 x 10^4 <= Re <= 1.2 x 10^5." Journal of Ocean Engineering, **38**: pp. 1713-1732.
21. Khalak, A. and Williamson, C.H.K., 1996, "Dynamics of a Hydroelastic Cylinder with Very Low Mass and Damping." Journal of Fluids and Structures, **10**: pp. 455-472.
22. Williamson, C.H.K., 1996, "Vortex dynamics in the cylinder wake." Annual Review of Fluid Mechanics, **36**: pp. 413-455.
23. Williamson, C.H.K. and Govardhan, R., 2004, "Vortex-induced vibrations." Annual Review of Fluid Mechanics, **36**: pp. 413 - 455.
24. Paidoussis, M.P., Price, S.J., and de Langre, E., *Fluid-Structure Interactions: Cross-Flow-Induced Instabilities*. 1 ed. 2010, Cambridge, UK: Cambridge University Press. 105-154.
25. Williamson, C.H.K. and Govardhan, R., 2004, "Vortex-induced vibrations." Annual Review of Fluid Mechanics, **36**: pp. 413-455.
26. Williamson, C.H.K. and Roshko, A., 1988, "Vortex formation in the wake of an oscillating cylinder." Journal of Fluids and Structures, **2**: pp. 355-381.
27. Bearman, P.W., 1984, "Vortex Shedding from Oscillating Bluff Bodies." Annual Review of Fluid Mechanics, **16**: pp. 195-222.
28. Sarpkaya, T., 1979, "Vortex-Induced Oscillations: A Selective Review." Journal of Applied Mechanics, **46**: pp. 241-258.
29. Bearman, P.W., 1984, "Vortex shedding from oscillating bluff bodies." Annual Review of Fluid Mechanics, **16**: pp. 195-222.
30. Lobo, V.M., 2012, "Design of a vortex induced vibration based marine hydro-kinetic energy system", MS Thesis, Missouri University of Science and Technology,
31. Vinod, A., 2012, "Enhancement of Vortex Induced Vibration using Roughness Strips", MS Thesis, Missouri University of Science and Technology,
32. http://thesis.library.caltech.edu/4684/1/JTK-Thesis(double-sided-printing).pdf, "PhD Dissertation, Klamo, J.T."
33. Raghavan, K., 2007, "Energy Extraction from a Steady Flow Using Vortex Induced Vibration", PhD Dissertation, University of Michigan, Ann Arbor
34. Khalak, A. and Williamson, C.H.K., 1997, "Fluid forces and dynamics of a hydroelastic structure with very low mass and damping." Journal of Fluids and Structures, **11**: pp. 973-982.
35. Blevins, R.D., *" Flow Induced Vibrations", Krieger Publishing Company, Malabar, Florida,*. 1994.
36. Jubran, B.A., Hamdan, M.N., and Al Bedoor, B.O., 1992, "Roughness and turbulence intensity effects on the induced flow oscillation of a Circular Cylinder." Appled Scientific Research, **49**: pp. 101-115.
37. Nishimura, H. and Taniike, Y., 2001, "Aerodynamic Characteristics of Fluctuating Forces on a Circular Cylinder." Journal of Wind Engineering and Industrial Aerodynamics, **89**: pp. 713-723.
38. Achenbach, E., 1968, "Distribution of Local Pressure and Skin Friction around a Circular Cylinder in Cross Flow up to Re = 5 x 10^6." Journal of Fluid Mechanics, **34**: pp. 625-639.
39. Lee, T. and Basu, S., 1997, "Nonintrusive measurements of the boundary layer developing on a single and two circular cylinders." Experiments in Fluids, **23**: pp. 187-192.
40. Son, J. and Hanratty, T.J., 1969, "Velocity Gradients at the Wall for flow around a cylinder at Reynolds numbers from 5 x 10^3 to 10^5." Journal of Fluid Mechanics, **35**: pp. 353-368.
41. Ballengee, D. and Chen, C.F. "Experimental determination of the separation point of flow around a circular cylinder"1971. in *Proceedings of ASME Fluids Engineering Conference on Flow Characteristics*. Instrument Society of America, Pittsburgh.
42. Roshko, A., 1961, "Experiments on the Flow Past a Circular Cylinder at Very High Reynolds Number." Journal of Fluid Mechanics, **10**: pp. 345-356.
43. Park, H., Bernitsas, M.M., and Ajith Kumar, R., 2012, "Selective Roughness in the Boundary Layer to Suppress Flow-Induced Motions of Circular Cylinder at 30,000<Re<120,000." Journal of Offshore Mechanics and Arctic Engineering, **134**: pp. 041801-041801.
44. Bianchi, N., Bolognani, S., Dalla Corte, D., and Tonel, F., 2003, "Tubular linear permanent magnet motors: an overall comparison." IEEE Transactions on Industry Applications, **39**: pp. 466-475.
45. Xinping, C., Chiang, W.-J., Ya-Chin, K., and Yi-Kuen, L., 2007, "Electromagnetic Energy Harvesting Circuit With Feedforward and Feedback DC–DC PWM Boost Converter for Vibration Power Generator System." Power Electronics, IEEE Transactions on, **22**: pp. 679-685.
46. Elmes, J., Gaydarzhiev, V., Mensah, A., Rustom, K., Shen, J., and Batarseh, I. "Maximum Energy Harvesting Control for Oscillating Energy Harvesting Systems"2007. in *Power Electronics Specialists Conference, 2007. PESC 2007. IEEE*.
47. Paing, T.S. and Zane, R. "Resistor Emulation Approach to Low-Power Energy Harvesting"2006. in *Power Electronics Specialists Conference, 2006. PESC '06. 37th IEEE*.
48. Esram, T. and Chapman, P.L., 2007, "Comparison of Photovoltaic array maximum power point tracking techniques." IEEE Transactions on Energy Conversions, **22**: pp. 439-449.